Transition metal contacts to graphene

Maria Politou, Inge Asselberghs, Iuliana Radu, Thierry Conard, Olivier Richard, Chang Seung Lee, Koen Martens, Safak Sayan, Cedric Huyghebaert, Zsolt Tokei, Stefan De Gendt, and Marc Heyns

Citation: Applied Physics Letters **107**, 153104 (2015); doi: 10.1063/1.4933192
View online: http://dx.doi.org/10.1063/1.4933192
View Table of Contents: http://scitation.aip.org/content/aip/journal/apl/107/15?ver=pdfcov
Published by the AIP Publishing

Transition metal contacts to graphene

Maria Politou,[1,2,a)] Inge Asselberghs,[2] Iuliana Radu,[2] Thierry Conard,[2] Olivier Richard,[2] Chang Seung Lee,[3] Koen Martens,[2] Safak Sayan,[2,4] Cedric Huyghebaert,[2] Zsolt Tokei,[2] Stefan De Gendt,[1,2] and Marc Heyns[1,2]
[1]*KU Leuven, 3001 Leuven, Belgium*
[2]*imec, Kapeldreef 75, 3001 Leuven, Belgium*
[3]*SAIT, Samsung Electronics Co., Suwon 443-803, South Korea*
[4]*Intel Corporation, 2200 Mission College Blvd, Santa Clara, California 95054, USA*

(Received 19 July 2015; accepted 30 September 2015; published online 15 October 2015)

Achieving low resistance contacts to graphene is a common concern for graphene device performance and hybrid graphene/metal interconnects. In this work, we have used the circular Transfer Length Method (cTLM) to electrically characterize Ag, Au, Ni, Ti, and Pd as contact metals to graphene. The consistency of the obtained results was verified with the characterization of up to 72 cTLM structures per metal. Within our study, the noble metals Au, Ag and Pd, which form a weaker bond with graphene, are shown to result in lower contact resistance (Rc) values compared to the more reactive Ni and Ti. X-ray Photo Electron Spectroscopy and Transmission Electron Microscopy characterization for the latter have shown the formation of Ti and Ni carbides. Graphene/Pd contacts show a distinct intermediate behavior. The weak carbide formation signature and the low Rc values measured agree with theoretical predictions of an intermediate state of weak chemisorption of Pd on graphene. © *2015 AIP Publishing LLC*.
[http://dx.doi.org/10.1063/1.4933192]

Graphene has emerged as one of the promising candidates for post-Si electronics, both for channel (Logic, RF, sensors) and interconnect applications. Regardless of the final application, graphene contact engineering is key for performance. Contact resistance (Rc) contributes significantly to the overall device resistance. Especially for aggressively scaled devices, Rc can be an important limiting factor. Therefore, the interaction between metal contacts and graphene, as well as the resulting Rc values, are important parameters for graphene device performance and for hybrid graphene/metal interconnects.

Reported Rc values depend on the metal used, the graphene type (exfoliated, CVD grown, epitaxially grown), the type of contact (top or side contact), the fabrication and post-fabrication treatments applied, the metal quality, and the interface cleanliness. Reported $Rc*W$ resistivity values show large scatter ranging from tens of kilo-ohms per μm down to few hundred ohms per μm for various metals and contact architectures.[1–23] Among the lowest values, $Rc*W$ of $185\pm20\,\Omega\,\mu$m is reported for exfoliated graphene and Pd contacts.[1] $Rc*W\sim100\,\Omega\,\mu$m is reported for exfoliated graphene sandwiched between boron nitride layers with Cr/Pd/Au edge contacts,[18] showing that the fabrication of edge contacts can be promising for the Rc decrease. Finally $Rc*W$ values below $100\,\Omega\,\mu$m have been recently reported when using highly pure Pd contacts.[23]

The transport behavior of the contacts is determined by the metal selection. The properties of graphene are altered by the metal contact. In theoretical studies,[24–26] two distinct cases are described. Metals such as Ni, Co, Ru, and Ti are expected to chemisorb on the graphene lattice. In this case, the d orbitals of the metals are strongly interacting with the graphene π orbitals. The graphene band structure is not preserved, but a gap opens where hybridized states appear. Metals such as Ag, Cu, Cd, Ir, Pt and Au, are characterized by more stable d orbital configurations and therefore are expected to physisorb on graphene. The outer shell s orbitals of the metals are interacting with the graphene π orbitals via a combination of van der Waals attraction and Pauli exclusion repulsion, forming dipoles at the graphene/metal interface. This is a weak interaction, characterized by preservation of the characteristic conical band structure of graphene. For the physisorbed metals, charge transfer will occur between graphene and metal resulting in a shift of the graphene cone and inducing n or p doping. The type and the amount of doping depend on the workfunction difference between graphene and metal. The formation of dipoles at the interface will also affect doping as it will result in an additional potential step. A particular case is Pd. According to some studies, it is expected to chemisorb on graphene in a similar way to Ni, Co, Ru, and Ti.[24–26] However, other studies report that Pd rather exhibits an intermediate mixed character of weak chemisorption.[27–30] The band structure of graphene is altered, but a weaker bonding occurs as compared to the case of the other chemisorbing metals.

In this work, we are extracting statistical electrical data over large device datasets for five representative contact metals, Ag, Au, Ni, Ti, and Pd. All the devices are fabricated on blanket CVD (Chemical Vapor Deposition) grown graphene samples ($2\times2\,\text{cm}^2$) by a single photolithography step and metal lift-off. Although exfoliated graphene is still of the highest quality, synthetic graphene is upscalable and thus the most relevant for practical applications. After electrical characterization, the metal/graphene interface is probed by X-ray Photo Electron Spectroscopy (XPS) and Transmission Electron Microscopy (TEM). Details on fabrication and

a)Electronic mail: Maria.Politou@imec.be

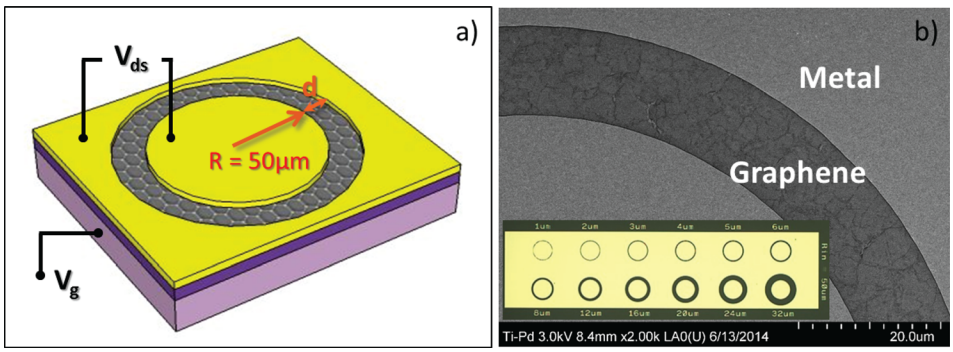

FIG. 1. (a) Schematic representation and (b) SEM micrograph of an individual cTLM device. The inset in (b) is an optical microscope picture of one cTLM structure consisting of 12 circular electrode configurations (inner and outer) with electrode spacing ranging from 1 μm up to 32 μm. The radius (R) of the inner electrode is 50 μm. Each processed sample consists of 72 structures.

characterization are given in the supplementary material.[31] The selected metals are commonly employed contact metals and are representative metals of different workfunctions and different metal/graphene bond strengths. 50-nm of Au and Pd are deposited while Ti, Ni, and Ag (30 nm) are capped with 20 nm Pd. All the metals are deposited by evaporation at a background pressure of 10^{-6} mbar.

Contact (Rc) and sheet resistance (Rs) values are extracted via the circular Transfer Length Method (cTLM).[32,33] Due to the circular configuration, current spreading effects are limited. In Figure 1, a schematic representation, a SEM, and an optical image of the structures are given. For the Rc extraction, I_{ds}–V_{ds} curves were measured at room temperature (25 °C) and at zero back-gate voltage V_g. Before measuring, all samples were annealed at 150 °C in N_2 for 1 h to reduce the effect of surface doping from ambient conditions (supplementary material Figure S1).

Cumulative distribution function (CDF) plots are made for each contacting metal in Figure 2, clearly visualizing the distribution of $Rc * W$ values from up to 72 structures across the sample. $Rc * W$ is the normalized Rc by the contact width W ($W = 2\pi R$). Three distinct regions are observed. The lower average $Rc * W$ values in the order of 3–5 kΩ μm are found for the noble metals, Ag, Pd, and Au. Ni results in an average value $Rc * W \sim 9$ kΩ μm and average $Rc * W \sim 48$ kΩ μm is measured for Ti contacts. The distribution of $Rc * W$ values measured for every metal is narrow with an exception in the case of Ti. Sheet resistance values span between 1 kΩ and 3 kΩ for all the samples (supplementary material Figure S2).

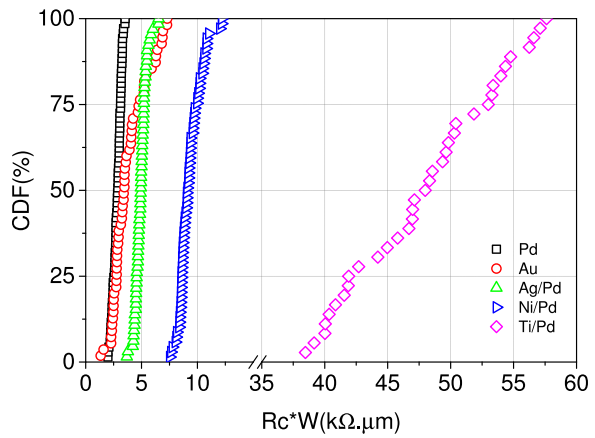

FIG. 2. CDF plots of contact resistivity $Rc * W$ visualizing the distribution of $Rc * W$ values across the samples. Lower values are obtained for Pd, Au, and Ag. Slightly higher values are obtained for Ni and very high values of $Rc * W$ are measured for the Ti contact. The spread of values is also larger for the Ti sample compared to the other metals.

For further in-depth understanding, we use Angle Resolved X-ray Photo Electron Spectroscopy (ARXPS) to characterize the metal/graphene interface for Ti, Ni, and Pd. In order to obtain information about the interface, several sputter steps were applied. As soon as the survey scans picked up a carbon signal, detailed XPS measurements were executed at that point. Further sputtering was omitted to limit damage to the graphene layer. An exit angle of 22° (measured from the normal of the sample) will give details of the graphene/metal interface, whereas an exit angle of 78° will give details closer to the surface. In order to reduce sputtering time and limit roughness formation due to sputtering, metal contacts of only 10 nm were deposited for the XPS study. After observing strong oxidation for Ti (supplementary material Figure S3), thicker contacts of 30 nm Ti capped with 20 nm Pd were examined for that case.

The XPS spectra of Ti/Pd (30 nm/20 nm), Ni/Pd (10 nm/10 nm), and Pd (10 nm) contacts are shown in Figure 3. For the Ti samples, apart from the Ti metallic double peak (Figure 3(a)) at ~455 eV and ~461 eV, we also observe the formation of Ti carbide at the graphene/Ti interface (Figure 3(b)) manifested with a strong peak at ~282 eV of the C1s scan. Contrary to the thin samples (supplementary material Figure S3), no signature of strong oxidation is present in the case of thick capped Ti. Within the XPS detection limits, only a small Ti oxide component can be observed (Figure 3(a)).

For the sample with the Ni contacts, apart from the metallic Ni peak at ~852 eV (Figure 3(c)), the formation of Ni carbide is observed at the graphene/Ni interface (Figure 3(d)) manifested as a tail at the low binding energy side of the C-C peak at ~284 eV. Regarding the Pd contacts (Figures 3(e) and 3(f)), we observe the metallic Pd peak and only a very subtle indication of carbide formation (peak broadening towards the low binding energies). Evidence of PdC formation between graphene and Pd observed by XPS has also been reported in the works of Ito *et al.*[34] and Gong *et al.*[35]

TEM and Energy Dispersive Spectroscopy (EDS) characterizations were additionally performed for Ti and Ni samples. The results for the Ti/Pd (30 nm/20 nm) sample are shown in Figure 4. In the results of Figures 4(b) and 4(c), we clearly observe an oxide layer (plateau in red color data, inverse triangles) at the Ti/graphene interface (full scan available in supplementary material Figure S4). As no sign

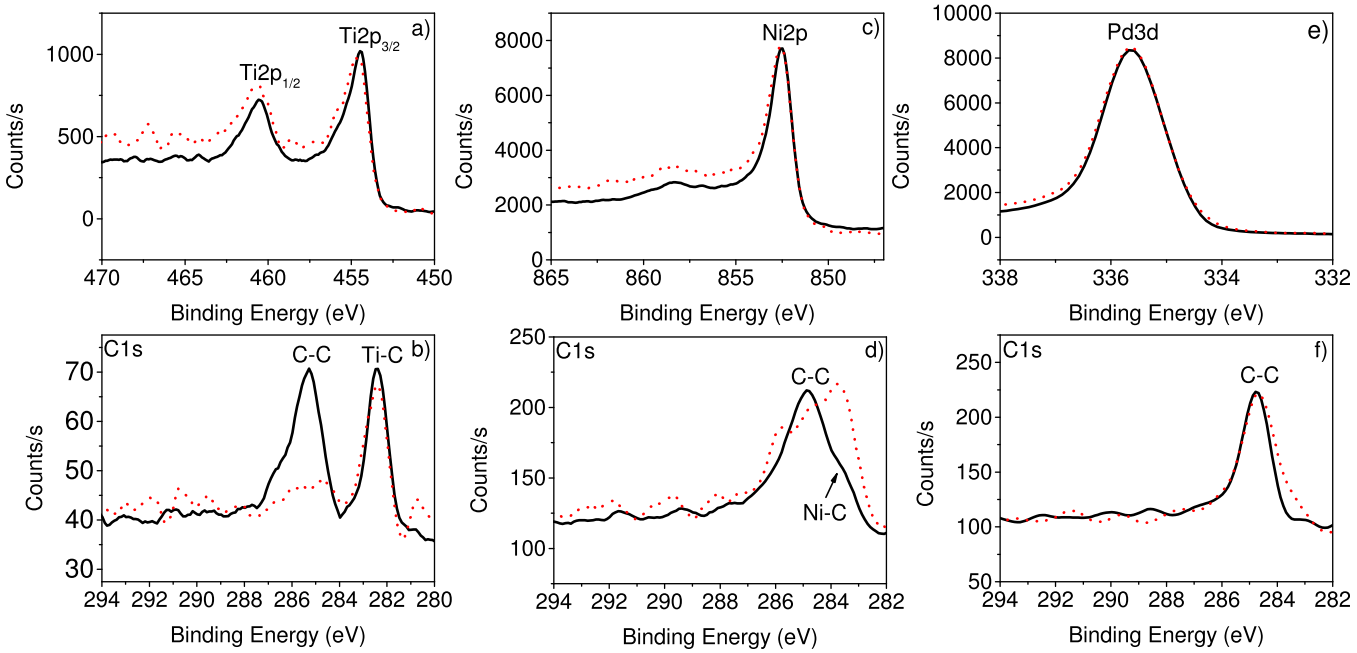

FIG. 3. XPS spectra of Ti ((a) and (b)), Ni ((c) and (d)) and Pd ((e) and (f)). The black solid line shows the measurements at 22° (interface), whereas the red dotted line shows the measurements at 78° (surface). Carbide formation is clearly observed in the Ti and Ni case. For the Pd case, the metallic Pd peak is observed with only a subtle indication of carbide formation within the XPS detection limits.

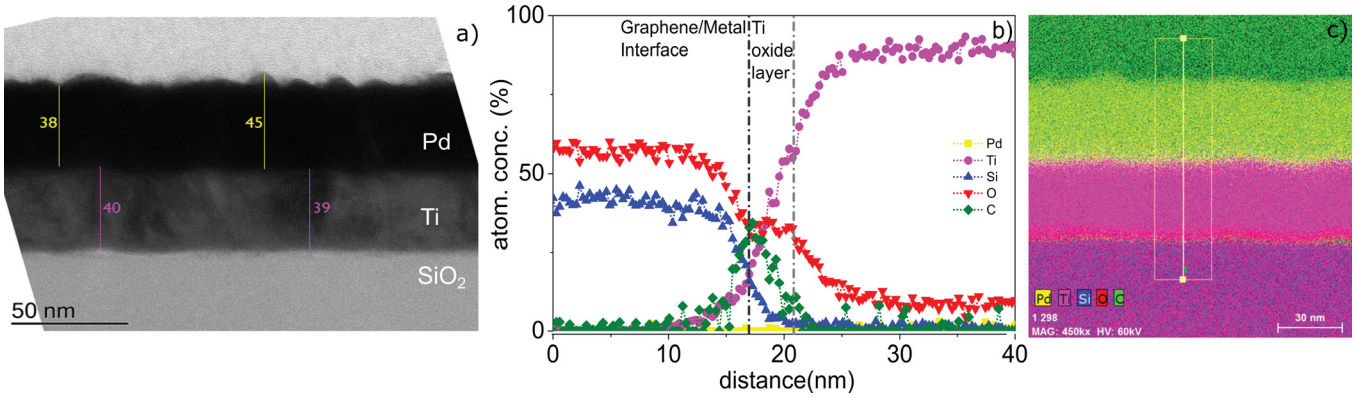

FIG. 4. (a) TEM and (b) and (c) EDS Data of the Ti/Pd sample. An oxide layer can be identified by EDS at the metal graphene interface. As no Si is present there, we assume that Ti oxide is forming above the interface.

of Si (blue triangles) is present at the interface and the layer appears to be above the graphene layer (green diamonds), we assume that this is a Ti oxide layer forming rather than the underlying SiO_2 signature. No such layer is present in the Ni/Pd case (supplementary material Figure S5). We also assume that the oxide is not an artefact of the TEM preparation as the simultaneous presence of Ti-O and Ti-C already during metallization has been reported before.[36,37] In an atmosphere where oxygen residuals are still present, Ti is observed to preferentially bind first with oxygen and subsequently with carbon, leading to TiC formation. The metallic Ti-Ti bond is reported to form last. A rough Pd surface is additionally observed with TEM (Figure 4(a)). A rough starting surface and the several sputtering steps can be a reason why the Ti oxide layer is not detected at the graphene/Ti interface by XPS in Figure 3(a), but only a slight surface oxidation is observed at the surface scan (78°). Several layers may be present simultaneously at the point of measurement a fact that can hinder the exact location of the detected oxide.

Table I summarizes all observations. The more inert metals (Ag, Pd, Au) show significantly lower contact resistance compared to the more reactive metals for which metal carbide formation is measured (Ni, Ti) at the interface. The Ti case is somewhat special, as a clear Ti oxide layer is observed above the metal/graphene interface. In Figure 5, we

TABLE I. Electrical and physical characterization results.

Metal	Bond	W_F (eV)[a]	$Rc * W$ (kΩ μm)[b]	Physical characterization
Pd	Chem.[c]	5.12	2.8 ± 0.4	Very weak carbide
Au	Phys.[d]	5.1	3.9 ± 1.5	No carbide
Ag	Phys.	4.26	5.0 ± 0.5	No carbide
Ni	Chem.	5.15	9.3 ± 1.0	Ni-C
Ti	Chem.	4.33	48.0 ± 5.7	Ti-C, Ti-O

[a]Metal workfunction.[38]
[b]Average values.
[c]Chem.: Chemisorbed.
[d]Phys.: Physisorbed.

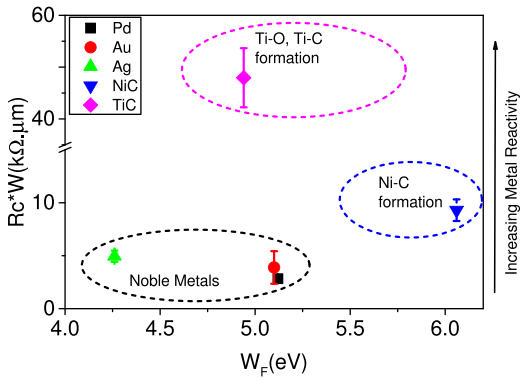

FIG. 5. Obtained $Rc * W$ values vs. workfunction and increasing metal reactivity. A clear trend can be observed correlating the high Rc values measured with the most reactive metals (Ni, Ti).

plot the obtained $Rc * W$ values vs. workfunction values.[38,39] Because of the observed carbides, the reported TiC and NiC workfunctions are used. The tendency for carbide formation can be rationalized considering their Gibbs free energy ΔG. It holds that $\Delta G_{TiC} < \Delta G_{Ni3C}$. In addition, Au and Ag are known to form highly unstable carbides,[40] therefore less likely to occur. The observed behavior is consistent with the location of the metals in the periodic table and the periodic trends. All metals under study are transition metals. Ti ($[Ar]3d^2 4s^2$) of group 4 takes part to bond formation more eagerly. Ni ($[Ar]3d^8 4s^2$) follows in group 10. Finally, all transition metals that show lower Rc have full d orbitals (Pd: $[Kr]4d^{10}$, Ag: $[Kr]4d^{10}5s^1$ and Au: $[Xe]4f^{14}5d^{10}6s^1$). However, in comparison with Ag and Au, Pd has no half-filled s orbital. A clear trend can be observed correlating the high Rc values measured with the most reactive metals (Ni, Ti). Especially, for the case of Ti, Rc values of 5–10 times higher were measured, compared to the rest of the metals. Since the TiC formation has been reported to improve the contact resistance,[34] the high Rc observed in our samples and the large spread in values are correlated with the presence of the oxide forming a barrier layer between the Ti-metal and the C-lattice and therefore screening the contact. The presence of the oxygen is difficult to avoid, and, since Ti is known as an oxygen getter,[41] this markedly shows the impact of the processing parameters on graphene device performance.

Among the investigated contact metals, low Rc values are obtained for the physisorbed metals (Ag, Au), whereas the chemisorbing Ni and Ti result in higher Rc. A distinct behavior is observed for Pd. From theory, the band structure of graphene under Pd is expected to change, similar to Ti and Ni. However, Pd results in low Rc similar to the physisorbed Ag and Au. In addition, within our XPS study, Pd shows only a weak indication of carbide formation contrary to Ni and Ti where the Ni and Ti carbide signature is prominent. Our experimental results, thus, agree with the theoretical predictions that the Pd/graphene interaction is a weak chemisorption of "mixed" character. Pd has demonstrated good performance as contact to graphene in various works.[1,2,9,16,23] In addition, Pd and Pt are modeled by means of first-principle calculations in the work of Wang and Che,[42] where a distinctly different behavior is reported for the two metals. Due to the necessary strain for Pd to match the graphene lattice, it is argued that an exchange transfer mechanism is triggered that results in increased interaction states and transmission channels for Pd contacts, allowing enough π electrons into the graphene. Results that support an enhanced performance of the Pd/C system are also reported in the work of Truong-Phuoc *et al.*[43]

Comparing the two physisorbed metals (Ag, Au), we observe that Ag shows slightly higher Rc than Au. In the theoretical study of Giovannetti *et al.*,[24] the same two metals are compared, and it is found that for larger equilibrium distances Au is expected to dope the graphene more compared to Ag, since for the corresponding Fermi energy shifts (ΔE_F) it holds $\Delta E_{F,Ag} < \Delta E_{F,Au}$ ($W_{F,graphene} \sim 4.5$eV). The lower doping of Ag compared to Au can explain the slightly higher observed Rc.

In summary, we have used the circular TLM over large device datasets to study the contact resistance Rc from a set of metals Ag, Au, Ni, Ti, and Pd to graphene. Within our study, the noble metals Au, Ag, and Pd, which form a weaker bond with graphene, are shown to result in lower Rc values compared to the more reactive Ni and Ti. XPS and TEM characterizations for the latter have shown the formation of Ti and Ni carbides. A distinct behavior is observed for Pd. Our XPS study shows only slight indication of Pd carbide formation, and a low Rc is measured electrically yielding similar values as for graphene Ag and Au contacts. Our results are in agreement with the theoretical predictions of an intermediate state of "weak chemisorption" of Pd on graphene.

All members of the Graphene and 2D Materials Team of imec, Belgium, are greatly acknowledged for their help and fruitful discussions. This work was supported by the imec Industrial Affiliation Program. K.M. acknowledges the Fund for Scientific Research (FWO), Belgium, for funding.

[1]F. Xia, V. Perebeinos, Y.-M. Lin, Y. Wu, and P. Avouris, Nat. Nanotechnol. **6**, 179 (2011).
[2]S. M. Song, J. K. Park, O. J. Sul, and B. J. Cho, Nano Lett. **12**, 3887 (2012).
[3]E. Watanabe, A. Conwill, D. Tsuya, and Y. Koide, Diamond Relat. Mater. **24**, 171 (2012).
[4]B.-C. Huang, M. Zhang, Y. Wang, and J. Woo, Appl. Phys. Lett. **99**, 032107 (2011).
[5]A. Venugopal, L. Colombo, and E. M. Vogel, Appl. Phys. Lett. **96**, 013512 (2010).
[6]K. Nagashio, T. Nishimura, K. Kita, and A. Toriumi, Appl. Phys. Lett. **97**, 143514 (2010).
[7]S. Russo, M. Craciun, M. Yamamoto, A. Morpurgo, and S. Tarucha, Phys. E **42**, 677 (2010).
[8]J. S. Moon, M. Antcliffe, H. C. Seo, D. Curtis, S. Lin, A. Schmitz, I. Milosavljevic, A. A. Kiselev, R. S. Ross, D. K. Gaskill, P. M. Campbell, R. C. Fitch, K.-M. Lee, and P. Asbeck, Appl. Phys. Lett. **100**, 203512 (2012).
[9]O. Balci and C. Kocabas, Appl. Phys. Lett. **101**, 243105 (2012).
[10]W. Li, C. A. Hacker, G. Cheng, Y. Liang, B. Tian, A. R. Hight Walker, C. A. Richter, D. J. Gundlach, X. Liang, and L. Peng, J. Appl. Phys. **115**, 114304 (2014).
[11]J. A. Robinson, M. LaBella, M. Zhu, M. Hollander, R. Kasarda, Z. Hughes, K. Trumbull, R. Cavalero, and D. Snyder, Appl. Phys. Lett. **98**, 053103 (2011).
[12]T. Kwon, H. An, Y.-S. Seo, and J. Jung, Jpn. J. Appl. Phys. **51**, 04DN04 (2012).
[13]Y. Matsuda, W.-Q. Deng, and W. A. Goddard, J. Phys. Chem. C **114**, 17845 (2010).
[14]J. T. Smith, A. D. Franklin, D. B. Farmer, and C. D. Dimitrakopoulos, ACS Nano **7**, 3661 (2013).

[15]W. S. Leong, H. Gong, and J. T. L. Thong, ACS Nano **8**, 994 (2014).
[16]S. Min Song, T. Yong Kim, O. Jae Sul, W. Cheol Shin, and B. Jin Cho, Appl. Phys. Lett. **104**, 183506 (2014).
[17]T. Chu and Z. Chen, ACS Nano **8**, 3584 (2014).
[18]L. Wang, I. Meric, P. Y. Huang, Q. Gao, Y. Gao, H. Tran, T. Taniguchi, K. Watanabe, L. M. Campos, D. A. Muller, J. Guo, P. Kim, J. Hone, K. L. Shepard, and C. R. Dean, Science **342**, 614 (2013).
[19]A. Franklin, S.-J. Han, A. Bol, and V. Perebeinos, IEEE Electron Device Lett. **33**, 17 (2012).
[20]A. Hsu, H. Wang, K. K. Kim, J. Kong, and T. Palacios, IEEE Electron Device Lett. **32**, 1008 (2011).
[21]R. Ifuku, K. Nagashio, T. Nishimura, and A. Toriumi, Appl. Phys. Lett. **103**, 033514 (2013).
[22]J. Lee, Y. Kim, H.-J. Shin, C. Lee, D. Lee, C.-Y. Moon, J. Lim, and S. C. Jun, Appl. Phys. Lett. **103**, 103104 (2013).
[23]H. Zhong, Z. Zhang, B. Chen, H. Xu, D. Yu, L. Huang, and L. Peng, Nano Res. **8**, 1669 (2015).
[24]G. Giovannetti, P. A. Khomyakov, G. Brocks, V. M. Karpan, J. van den Brink, and P. J. Kelly, Phys. Rev. Lett. **101**, 026803 (2008).
[25]C. Gong, G. Lee, B. Shan, E. M. Vogel, R. M. Wallace, and K. Cho, J. Appl. Phys. **108**, 123711 (2010).
[26]K. T. Chan, J. B. Neaton, and M. L. Cohen, Phys. Rev. B **77**, 235430 (2008).
[27]M. Quiroga and G. Cabeza, Braz. J. Phys. **43**, 126 (2013).
[28]R. Mao, B. D. Kong, C. Gong, S. Xu, T. Jayasekera, K. Cho, and K. W. Kim, Phys. Rev. B **87**, 165410 (2013).
[29]Q. Ran, M. Gao, X. Guan, Y. Wang, and Z. Yu, Appl. Phys. Lett. **94**, 103511 (2009).
[30]R. Zan, U. Bangert, Q. Ramasse, and K. S. Novoselov, J. Phys. Chem. Lett. **3**, 953 (2012).
[31]See supplementary material at http://dx.doi.org/10.1063/1.4933192 for fabrication and characterization details and also for additional sheet resistance (*Rs*), XPS, TEM, and EDS data.
[32]D. K. Schroder, *Semiconductor Material and Device Characterization*, 3rd ed. (A Wiley-Interscience Publication, 2006).
[33]J. Klootwijk and C. Timmering, in *Proceedings of the International Conference on Microelectronic Test Structures, 2004, ICMTS'04* (IEEE, 2004), pp. 247–252.
[34]K. Ito, T. Ogata, T. Sakai, and Y. Awano, Appl. Phys. Express **8**, 025101 (2015).
[35]C. Gong, S. McDonnell, X. Qin, A. Azcatl, H. Dong, Y. J. Chabal, K. Cho, and R. M. Wallace, ACS Nano **8**, 642 (2014).
[36]W. P. Leroy, C. Detavernier, R. L. Van Meirhaeghe, A. J. Kellock, and C. Lavoie, J. Appl. Phys. **99**, 063704 (2006).
[37]A. Felten, I. Suarez-Martinez, X. Ke, G. Van Tendeloo, J. Ghijsen, J.-J. Pireaux, W. Drube, C. Bittencourt, and C. P. Ewels, ChemPhysChem **10**, 1799 (2009).
[38]H. B. Michaelson, J. Appl. Phys. **48**, 4729 (1977).
[39]H. Hugosson, O. Eriksson, U. Jansson, A. Ruban, P. Souvatzis, and I. Abrikosov, Surf. Sci. **557**, 243 (2004).
[40]S. Shatynski, Oxid. Met. **13**, 105 (1979).
[41]F. Cardarelli, *Materials Handbook: A Concise Desktop Reference*, 2nd ed. (Springer-Verlag, London Limited, 2008).
[42]Q. J. Wang and J. G. Che, Phys. Rev. Lett. **103**, 066802 (2009).
[43]L. Truong-Phuoc, C. Pham-Huu, V. Da Costa, and I. Janowska, Chem. Commun. **50**, 14433 (2014).